Design and Electromagnetic Simulation of Axial-Flux Hybrid-Excitation Motor for Electric Ship Propulsion

Chu Wang*[1, a1], Weiwei Geng [2, b]

[1]Ship Engineering, China Ship Scientific Research Center, Wuxi, Jiangsu Province, China;

[2]School of Automation, Nanjing University of Science and Technology, Nanjing, Jiangsu Province, China;

ABSTRACT

In this paper, a novel axial flux hybrid excitation motor (AFHEM) for electric ship propulsion system is proposed. On the basis of traditional axial flux permanent magnet motor (AFPMM), a new type of AFHEM was composed of field winding and magnetic flux ring, and adopting a dual rotor single stator topology structure. The unique outer magnetic ring and magnetic flux regulation principle of the proposed AFHEM were discussed, and finite element analysis was used to simulate and analyze the motor, including torque output capability, air-gap magnetic flux density, and risk analysis of permanent magnet demagnetization under different excitation currents. By adjusting the excitation current, the weak magnetic and overload capacity of the motor can be improved, and it has high torque output and magnetic field regulation ability.

Keywords: Hybrid excitation; axial-flux permanent magnet motor; propulsion motor; 3D finite element method; magnetic field regulation

1. INTRODUCTION

With the continuous development of modern technology and industry, environmental pollution and energy shortage have gradually attracted the attention of various countries [1]. In the field of ships, the development of new electric ships has become an important measure to reduce oil consumption, improve energy utilization efficiency, and improve marine environmental pollution in maritime transportation [2].

Improving the torque density of the propulsion motor and enhancing the combat maneuverability of ships has become one of the key technologies for the development of electric ship propulsion. The improvement of torque density can not only save a lot of space inside the ship, but also achieve greater torque output capacity, bringing stronger torque output function. In addition, the use of direct drive technology can eliminate the traditional mechanical transmission devices required [3].

Although the advantages of radial motors currently meet the requirements of electric ship propulsion systems[4], there are still significant challenges, such as the difficulty in coordinating high torque density and efficient operation over a wide speed range[5]、power output losses caused by high temperature or demagnetization of impact permanent magnets, making fault-tolerant operation difficult[6].

This article focuses on the key technology of a new AFHEM used for electric ship propulsion. A novel AFHEM with adjustable air gap magnetic field was designed, and the topology structure of the motor was theoretically studied, modeled, and simulated using Ansys Maxwell.

The design indicators of the propulsion motor are shown in Table 1.

[1*a] wangchu@njust.edu, [b] gww@njust.edu.cn

The International Conference Optoelectronic Information and Optical Engineering (OIOE2024), edited by Yang Yue, Lu Leng, Proc. of SPIE Vol. 13513, 135131U · © 2025 SPIE · 0277-786X · © The Authors. Published under a Creative Commons Attribution CC-BY 3.0 License · doi: 10.1117/12.3045582

Table 1. Design indicators of motors.

Parameters	
Peak torque	＞1000 N·m
Maximum speed	＞1500 r/min
Peak torque density	＞30 N·m/kg
DC Bus Voltage	540 V

2. DESCRIPTION AND PRINCIPLE OF THE MACHINE

2.1 Topology Structure

The basic topology of the new AFHEM motor proposed in this chapter is shown in Figure.1. The motor consists of dual rotors and a single stator. Based on the traditional dual rotor AFPMM, the rotor magnetic back yokes on both sides of the stator are extended radially, and a magnetic ring is added between the two rotor discs to connect the two rotor magnetic back yokes, forming an inverted U-shaped rotor structure; The excitation winding is set in the inverted U-shaped rotor cavity, located on the outer ring of the stator core. On both sides of the magnetic yoke, permanent magnets and iron core poles are installed in a staggered manner. The rotor disk is installed with one magnetic pole staggered in the axial direction, and the magnetization direction of the permanent magnets on the rotor disk is kept consistent. By serializing an electrically excited magnetic potential source in the axial magnetic circuit, bidirectional adjustment of the two axial air gap magnetic fields corresponding to the iron core poles is achieved.

2.2 Magnetic Flux Principle and Path

The main magnetic flux paths and directions inside the new AFHEM motor are shown in Figure 2. Adopting a magnetic flux through magnetic circuit, the magnetic pole itself has no polarity. By increasing the current excitation of the electric excitation winding, the magnetic poles are magnetized, which can be equivalent to traditional AFPMM. By adjusting the direction and magnitude of the excitation current, the air gap magnetic field of AFHEM can be adjusted. In zero excitation state, the magnetic flux generated by the permanent magnets on the two rotor discs forms coupling continuity on the stator yoke and a closed loop is formed through the magnetic flux ring on the inverted U-shaped rotor. The motor design is shown in Table 2.

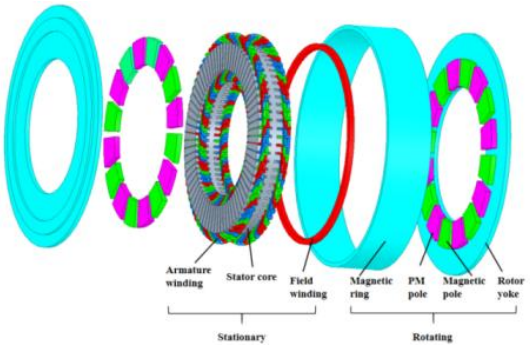

Figure 1. Explosive view of topology structure.

Table 2. Motor design.

Parameters		Parameters	
Outer diameter of stator	350mm	Inner diameter of stator	250mm
Number of stator slots	72	Number of rotor poles	16
Outer diameter of magnetic ring	446mm	Inner diameter of magnetic ring	430mm
Thickness of stator	64mm	Unilateral axial air gap length	1mm
Thickness of permanent magnet	10mm	Pole embrace	0.8
Thickness of rotor core	12mm	Thickness of magnetic guide ring	8mm
Stator core	B20AT1500	Winding	copper
PM pole	G52UH	Magnetic pole	SMC700

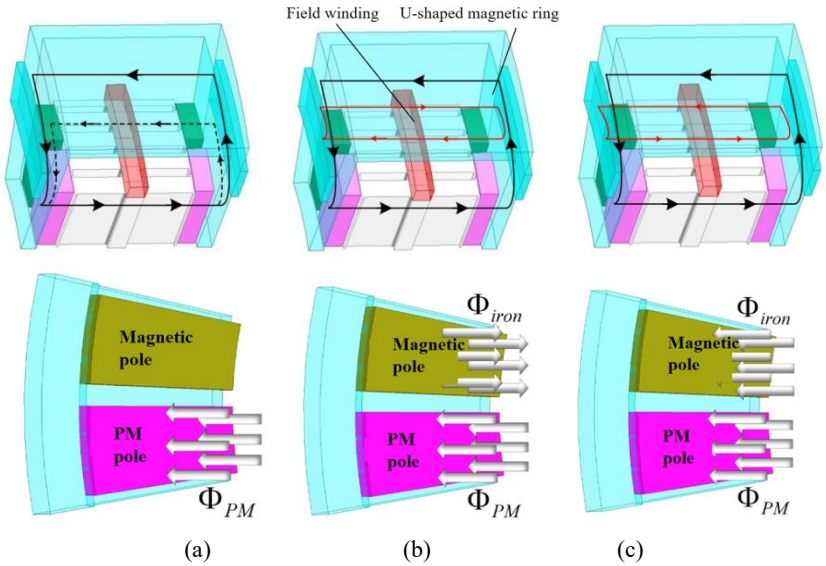

Figure 2. Magnetic flux paths of the AFHEM under different excitation current. (a) No excitation current. (b) Flux-strengthening. (c) Flux-weakening.

3. ANALYSIS OF SIMULATION RESULTS OF MOTORS

Figure 3 shows the magnetic field distribution cloud map of the motor under different excitation currents. It can be seen that when the excitation current is 0, most of the magnetic flux passes through the magnetic flux ring. A small portion of the magnetic flux passes through the stator teeth, as shown in Figure 3 (a). When the excitation current is positive, forward excitation is applied, as shown in Figure 3 (b). When the excitation current is negative, reverse excitation results in a relatively saturated magnetic flux ring, as shown in Figure 3 (c).

Figure 4 shows the no-load air gap magnetic flux density of the motor under different excitation currents. It can be seen from the Figure that the motor has good magnetic field regulation ability. When the excitation current is positive, the motor is in an increased magnetization state, and the direction of the electric excitation magnetic potential generated by the electric excitation winding is the same as that of the permanent magnet magnetic potential. When the excitation current is negative, the motor is in a demagnetized state, and the electric excitation magnetic potential generated by the electric excitation winding is opposite to the PM magnetic potential, playing a weak magnetic role.

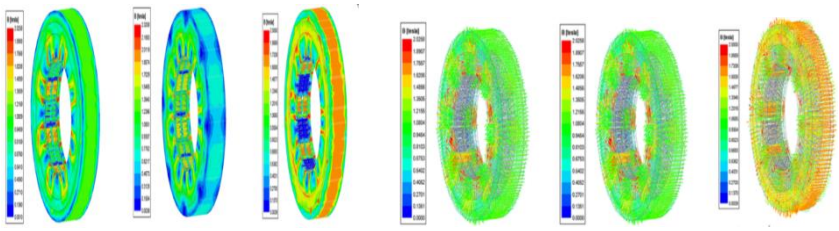

Figure 3. No-load field distributions and flux density under different excitation fields. (a) If=30A (b) If=0A (c) If=-30A.

The cogging torque of the motor under different excitation currents under no-load state was obtained through simulation, as shown in Figure 5.

The electromagnetic torque of the AFHEM as a function of field and armature currents are shown in Figure. 6. The torque versus current angle curve of AFHEM and AFPMM are compared in Figure.7.

By changing the magnitude of the armature current, the torque output characteristics of the motor under different excitation currents can be obtained, as shown in Figure 8. When the excitation current is 30A, the torque characteristics of the motor under different armature currents are shown in Figure 8 (a). When the excitation current is 0A, the

excitation winding does not receive any current, and the torque characteristics of the motor under different armature currents are shown in Figure 8 (b). Similarly, when the excitation current is -30A, the torque characteristics of the motor at different armature currents are shown in Figure 8 (c).

Figure 9 shows the magnetic field distribution cloud map of the motor under different excitation states under rated load conditions.

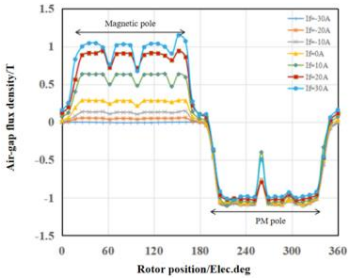

Figure 4. Axial air-gap flux density waveform under.

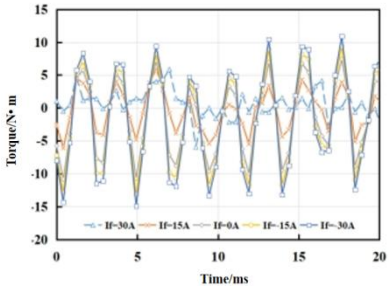

Figure 5. No-load cogging torque different field currents at no load. :

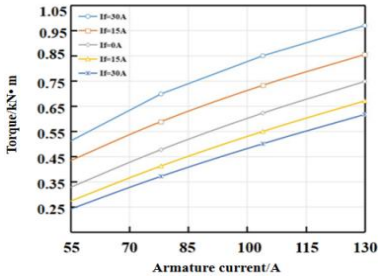

Figure 6. MTPA curves of AFHEM.

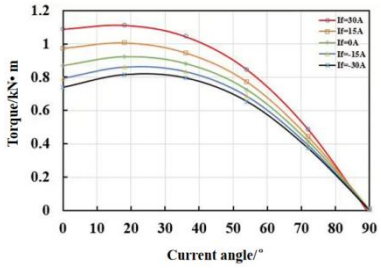

Figure 7. MTPA curves of the AFHEM and AFPMM.

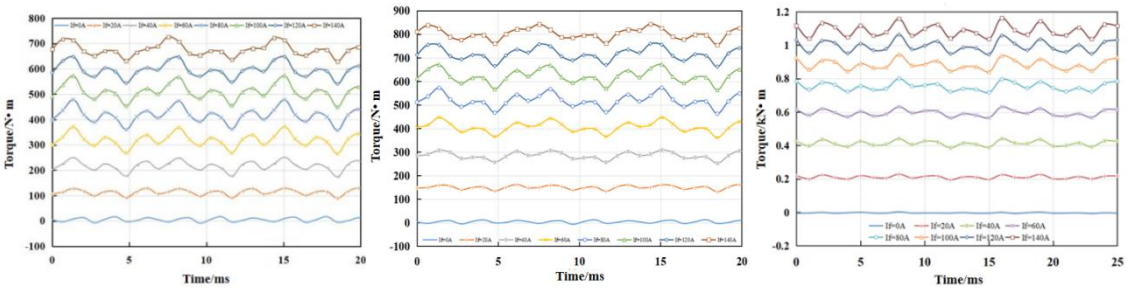

(a) (b) (c)

Figure 8. Torque output characteristics under different excitation fields. (a) If=-30A (b) If=0A (c) If=30A.

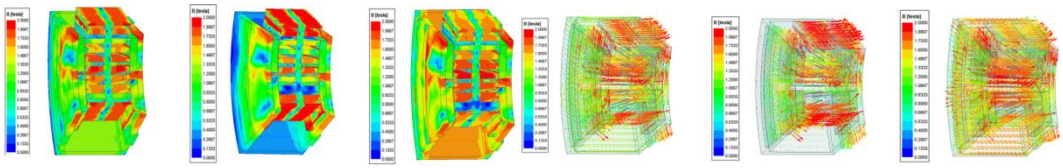

(a) (b) (c)

Figure 9. Magnetic field distribution and flux density under different excitation fields at rated-load (a) If=30A (b) If=0A (c) If=-30A.

Due to the introduction of excitation windings, the demagnetization risk of permanent magnets caused by excitation windings is also worth analyzing. The working environment of electric ship propulsion motors is harsh, often accompanied by extreme environments such as high temperature and impact vibration. Figure 10 shows the torque output of AFHEM under 30%, 50%, 70%, and 100% demagnetization of permanent magnets. When the demagnetization of the permanent magnet is not severe, as the armature current and excitation current increase, the motor can still output higher torque. Even when the permanent magnet is completely demagnetized, there is still a certain torque output.

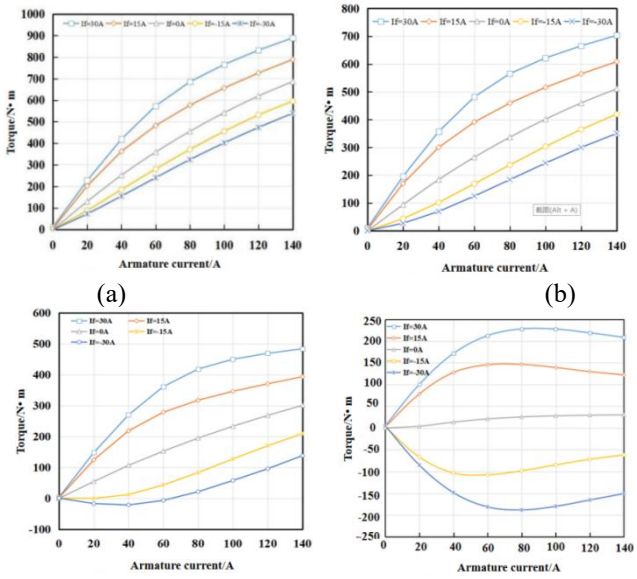

(a) (b)

(c) (d)

Figure 10. Torque output capacity after PM demagnetization: (a) Demagnetize by 30%. (b) Demagnetize by 50%. (c) Demagnetize by 70%. (d) Demagnetize by 100%.

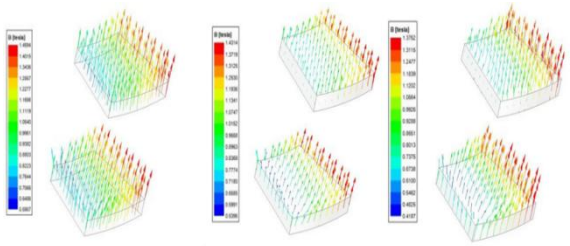

Figure 11. Simulate magnetic vector distribution during demagnetization of permanent magnets (a) If=30A (b) If=0A (c) If=-30A.

In extremely harsh conditions, motors are prone to the risk of demagnetization of permanent magnets. When the peak load occurs, the q-axis current suddenly disappears and the load current is only the d-axis current. The risk simulation of demagnetization of permanent magnets under weak magnetic conditions for armature current or excitation current is shown in Figure 11. Even under extreme conditions, the magnetic field distribution of permanent magnets does not reverse, with a minimum value of about 0.4T, indicating a low risk of demagnetization.

4. SUMMARY

This paper introduces the topology principle and magnetic flux path of the proposed AFHEM. Its effectiveness was verified through finite element analysis. Simulate the no-load and load characteristics of a motor under different excitation states, and the magnetic topology allows for bidirectional magnetic field regulation capability. It also verified the range of magnetic field regulation and torque output. It has been proven that hybrid excitation topology can easily control axial gap magnetic flux and has high power density, making it suitable for integrated applications of electric ship propulsion.

REFERENCES

[1] Fangxin Hou, Xiaotong Chen, Xing Chen, Fang Yang, Zhiyuan Ma, Shining Zhang, et al., "Comprehensive analysis method of determining global long-term GHG mitigation potential of passenger battery electric vehicles", Journal of cleaner production, vol. 289, pp. 125137, 2021

[2] Y. Hu, Z. Wang and X. Li, “Impact of policies on electric vehicle diffusion: An evolutionary game of small world network analysis’’, Journal of Cleaner Production, vol. 265, pp. 121703, 2020.

[3] McCarty F B.Hybrid excited generator with flux control of consequent-pole rotor：US，4656379A[P].1987-04-07.

[4] D. S. Yadav and M. Manisha, "Electric Propulsion Motors: A Comparative Review for Electric and Hybrid Electric Vehicles," 2022 IEEE International Conference on Distributed Computing and Electrical Circuits and Electronics (ICDCECE), Ballari, India, 2022, pp. 1-6, doi: 10.1109/ICDCECE53908.2022.9793099.

[5] Y. Yao and C. Liu, "A Efficient Nine-Phase PM Flux-Switchi0ng Machine with High Torque Density and Low Torque Ripple," 2018 Asia-Pacific Magnetic Recording Conference (APMRC), Shanghai, China, 2018, pp. 1-2, doi: 10.1109/APMRC.2018.8601110.

[6] Q. Zhou and L. Wang, "Simulation and Analysis of the Fault of Coreless Axial Flux Permanent Magnet Synchronous Motor," 2020 IEEE International Conference on Applied Superconductivity and Electromagnetic Devices (ASEMD), Tianjin, China, 2020, pp. 1-2, doi: 10.1109/ASEMD49065.2020.9276273.